JOURNAL OF PROPULSION AND POWER
Vol. 9, No. 3, May–June 1993

Experimental Supersonic Hydrogen Combustion Employing Staged Injection Behind a Rearward-Facing Step

John D. Abbitt III* and Corin Segal*
University of Florida, Gainesville, Florida 32611
and
James C. McDaniel,† Roland H. Krauss,‡ and Robert B. Whitehurst§
University of Virginia, Charlottesville, Virginia 22903

An experimental investigation of a Mach 2 combustor has been conducted in order to characterize flow properties in a supersonic reacting flowfield. Hydrogen was injected transversely as staged, underexpanded jets behind a rearward-facing step into a ducted Mach 2 air freestream. The effects of the chemical reaction on the supersonic flowfield was investigated using shadowgraphs, broadband flame emission photography, and planar laser-induced fluorescence of OH. The shadowgraphs indicated that the wave pattern in the combustor along with flowfield unsteadiness was strongly affected by the heat release. The broadband flame emission photographs revealed large regions of no combustion in the vicinity of the fuel injectors where fuel/air mixing was insufficient to support combustion. These regions decreased in size as the freestream stagnation temperature was decreased for fixed hydrogen mass flow rate, consistent with an increase in the effective *Q*-ratio with combustion. The size of the zones containing OH in the planar fluorescence images also increased as the main flow stagnation temperature was decreased. Reaction zones were found in the planar fluorescence images away from regions containing injectant in a nonreacting study of the same geometry, indicating that the pressure rise associated with the reaction forced a large redistribution of the fuel.

Introduction

AIR-BREATHING supersonic-combustion-ramjet (scramjet) engines are currently under active development for the propulsion of future hypersonic vehicles. The flowfield in the combustor of such an engine is complex, and presents a considerable challenge in developing a combustor geometry that promotes sufficient mixing of the air and injectant fuel so that the desired chemical reaction and thus, heat release, can occur within the residence time of the mixture. There are a number of factors that contribute to the difficulty in understanding supersonic reacting flowfields. One of these factors is the large variation in the velocity and thermodynamic variables. In addition, the finite rate kinetics are strongly coupled to the fluid mechanics which determine the heat release and pressure rise. Another complication results from the changes in the gas composition as the reaction proceeds.

In order to improve the current understanding of these flowfields, in-stream measurements of flowfield properties under simulated operating conditions are essential. This work represents the second phase of an experimental investigation of the flow characteristics of a supersonic combustor using transverse injection behind a rearward-facing step. This geometry has been the subject of considerable theoretical studies involving both reacting and nonreacting flowfields.[1,2] In the first phase of the experiment, spatially resolved, time-averaged measurements of fuel mixing, temperature, pressure, and velocity fields were made in the Mach 2 nonreacting combustor.[3,4] For this second phase, a wind tunnel was built in which hydrogen was injected into the Mach 2 freestream combustor and burned. The tunnel incorporates several features which permitted a number of unique experiments. The tunnel can operate continuously, meaning that tests requiring long run times could be performed. Stagnation conditions could be held within 1% of the set points for the duration of all the experiments. A clean, dry airflow could be obtained with stagnation temperatures as high as 800 K using electrical resistance heaters. Large quartz windows in the test section permitted the use of flow visualization to characterize the entire flowfield. Flow visualization techniques included planar laser-induced fluorescence, as well as shadowgraphs and film-based imaging of the broadband visible emission from the hydrogen-air flame.

Experiment

The flowfield used in this study is shown in Fig. 1. A continuous, shock-free Mach 2.0 freestream, provided by a two-dimensional Laval nozzle, is introduced into a rectangular

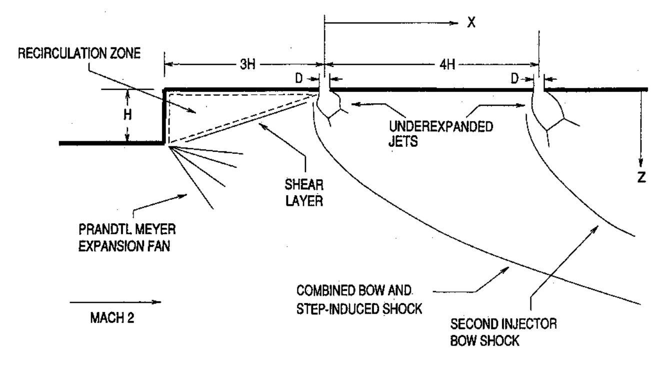

Fig. 1 Flowfield schematic diagram.

Received Nov. 4, 1991; presented as Paper 92-0090 at the AIAA 30th Aerospace Sciences Meeting, Reno, NV, Jan. 6–9, 1992; revision received Dec. 31, 1992; accepted for publication Dec. 31, 1992.

*Assistant Professor, Department of Aerospace Engineering, Mechanics and Engineering Science, 231 Aerospace Bldg. Member AIAA.

†Associate Professor, Department of Mechanical and Aerospace Engineering. Member AIAA.

‡Associate Research Professor, Department of Mechanical and Aerospace Engineering. Member AIAA.

§Research Scientist, Department of Mechanical and Aerospace Engineering. Member AIAA.

duct. Upon entering the duct, the flowfield accelerates and turns past a rearward-facing step through a Prandtl-Meyer expansion fan. The duct entrance is 3.81-cm wide and 3.04 cm in height, downstream of the step, which is 0.51-cm high. The step isolates the nozzle boundary layer from the pressure rise generated in the combustor and also helps to sustain combustion by providing a recirculation zone for the fuel-air mixture.

Hydrogen was injected for both the reacting and nonreacting studies through two staged injectors, each 1.0 mm in diameter. (Other injector diameters were also studied but are not reported herein.[5]) The injectors were located three step heights and seven step heights, respectively, downstream of the step. Staging of the injectors provides improved injectant penetration and mixing, and also provides a recirculation region between the injectors for additional flameholding.

A schematic diagram of the overall supersonic combustion wind-tunnel facility is shown in Fig. 2. Dry, high-pressure air is brought to the bottom of an 8.7-m-deep pit located beneath the floor of the building. Here, the air enters a series of tank sections which contain the electrical resistance heaters. At this point, the flow is at a relatively low velocity and at essentially stagnation conditions. The air then passes through a Laval nozzle, where it is accelerated to Mach 2, and into the rectangular test section. After leaving the test section, the air is exhausted through a pipe which extends through the roof of the building. The airflow is set by adjusting the stagnation pressure to a value that corresponds to a desired static pressure in the test section. For these tests, the stagnation pressure was nominally 60 psia.

One wall of the test section contains the hydrogen injector block which is made of nickel and is water cooled. The wall opposite the injector block is made of stainless steel with a large 10 cm × 2.5 cm fused silica observation window. The side walls were solid pieces of fused silica which extended the entire length of the test section.

The hydrogen-air mixture was ignited while the flow was subsonic. To start the combustion process, a hydrogen pilot feed was introduced into the base of the step through three small holes. The reaction was initiated by a spark source located in the base of the step. Once the reaction was established, the flow was slowly adjusted until supersonic conditions were achieved. The hydrogen pilot feeds were then turned off, and the combustor was fueled entirely by the main injectors. The mass flow rate of the hydrogen through the injectors was adjusted to provide a desired "Q-ratio," which is the ratio of the dynamic pressure at the sonic injector exit to that of the Mach 2 freestream. It is calculated using

$$Q = \frac{(\gamma_1/2)p_1M_1^2}{(\gamma_2/2)p_2M_2^2} \tag{1}$$

In this experiment, γ_1 and γ_2 were both 1.4, M_1 was 1.0, M_2 was 2.0, and p_1 and p_2 were static pressures calculated from the stagnation pressures using isentropic relations for quasi-one-dimensional flow at the given Mach number. The stagnation pressure of the hydrogen was converted to mass flow rate by assuming that the sonic injector had a discharge coefficient of unity.

The optical setup for the planar laser induced fluorescence study is shown in Fig. 3. Rotational transitions in the (1, 0) vibrational band of the OH $A^2\Sigma^+ \leftarrow X^2\Pi$ electronic system were excited by a sheet of laser light. The fluorescence that resulted as the OH radical decayed radiatively from the excited electronic states was observed with a gated (100-ns exposure time) light-intensified ultraviolet charge injection device (CID) video camera.

The laser source for this experiment was the 532-nm frequency-doubled output of a Nd:YAG laser which pumped a pulsed dye laser, tuned to a frequency corresponding to half that of a desired OH transition. The frequency was doubled again by passing the output from the dye laser through a birefringent KD*P crystal. The laser was calibrated prior to each run by passing the beam through an acetylene/air flame and comparing the observed fluorescence spectrum with a known spectrum. In addition to the calibration, the intensity distribution of the laser sheet was also measured.

As shown in Fig. 3, the beam was formed into a 100-μm thick sheet and directed through the test section. The fluorescence images were recorded using the CID camera. The sheet-forming optics and camera were mounted on motor-driven translation stages for remote positioning of the light

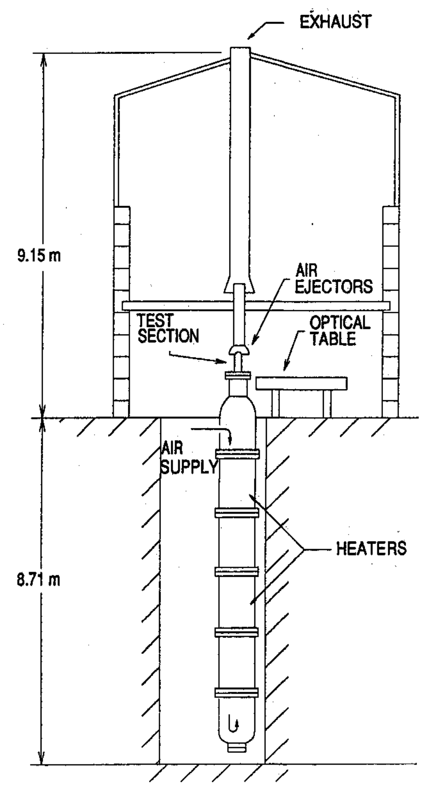

Fig. 2 Supersonic combustion wind-tunnel facility.

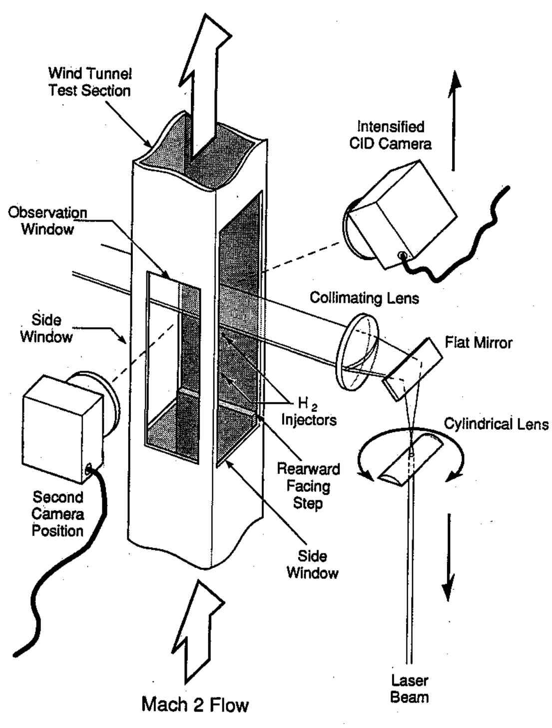

Fig. 3 Optical setup.

sheet. "Cross-sectional" images were obtained by orienting the laser sheet perpendicular to the injection wall and the flow direction. The viewing angle of the camera was set at 45 deg to the plane of the light sheet. Distortion of the aspect ratio of the image was corrected digitally. "Spreading" images were obtained by orienting the laser sheet parallel to the injection wall and imaging from the second camera position shown in Fig. 3. By traversing the laser sheet, a three-dimensional map of zones rich in OH was obtained.

Visible broadband emission images from the hydrogen-air flame were collected using a 35-mm camera with a remote shutter release and film transport mechanism. Shadowgraphs were obtained by passing an expanded beam from an argon ion laser through the flowfield onto a screen, and recorded with the 35-mm camera.

OH Laser-Induced Fluorescence Theory

The expression for the fluorescence signal induced by a broadband laser source is given by

$$S_f = CI(X)\frac{A_{21}}{A_{21} + Q + D}B_{21}F_1(T)N_0 \qquad (2)$$

where C is a system constant that includes the optical collection efficiency, $I(X)$ is the spatial distribution of the intensity of the incident laser light, A_{21} is the Einstein coefficient for spontaneous emission, or the radiative decay rate, B_{21} is the Einstein coefficient for absorption, Q is the collisional quenching rate, D is the predissociation rate, $F_1(T)$ is the Boltzmann population fraction of the ground state resonant with the laser, and N_0 is the total number density of the molecules being excited. When this equation is used to describe laser-induced OH fluorescence from excited $v' = 0$ or $v' = 1$ vibrational states, the predissociative rate term D disappears since it is several orders of magnitude smaller than either A_{21} or Q.

Under typical wind-tunnel conditions, A_{21} is much smaller than Q and is neglected in the denominator. B_{21} is a constant for a given transition and may be included in the constant term. The laser power can be measured, and is, thus, a known quantity where the beam enters the flowfield. $F_1(T)$ varies with temperature.[5] By selecting a transition where $F_1(T)$ is fairly insensitive to temperature, the fluorescence signal becomes proportional to the number density of the molecule and inversely proportional to Q.

The temperature dependence of the Boltzmann population fraction was minimized using the Q_16 transition of the (1, 0) vibrational band of the $A^2\Sigma^+ \leftarrow X^2\Pi$ electronic system. This transition has a high Boltzmann population fraction at this temperature and shows, in the expected temperature range, the least sensitivity to temperature. The (1, 0) vibrational band also is located in a portion of the spectrum which allows the use of a dye in the dye laser with the highest gain. Use of this transition did result in appreciable beam absorption causing a systematic error in $I(X)$. Visualization was attempted using weaker transitions where less absorption was expected, but the fluorescence intensity at these wavelengths was below the sensitivity of the camera. Techniques to minimize the effects of laser beam absorption are discussed later. A systematic error in the fluorescence signal S_f also results from radiative, or fluorescence, trapping. This effect is reduced when the camera is oriented to obtain spreading images since the region containing OH through which the photons must pass is relatively small. The region through which the photons must pass when the camera is oriented to obtain cross-sectional images, however, is rich in OH, and the trapping effect is significant. Furthermore, it is asymmetric, and results in an apparent reduced concentration of OH on the side of the test section away from the camera.

Results

Shadowgraphs

In Fig. 4, shadowgraphs of the test section obtained through the side windows are presented. In each shadowgraph, the nozzle exit Mach number is 2, the Q-ratio is 1.5, and the stagnation temperature is about 650 K. In Fig. 4a, the flowfield is nonreacting, while in Fig. 4b, the flowfield is reacting. In these images, the flow is from left to right, and hydrogen injection is from the top, behind the rearward-facing step. Arrows indicate hydrogen injection points. Two waves protruding at a 30-deg angle to either wall are seen at the entrance to the test section. These waves are created by a slight misalignment at the point where the test section is attached to the nozzle. These are very weak waves, as indicated by the Mach angle (30 deg at Mach 2) they form with the wall, and their effect on the flowfield is negligible. At the step on the left side of the image shown in Fig. 4a, the flow accelerates through the Prandtl-Meyer expansion fan attached to the step. Hydrogen is introduced into the test section through the two injectors located three step heights and seven step heights, respectively, downstream of the step. At the injector points, two barrel shocks can be seen penetrating into the flow. The barrel shocks from both injectors appear to penetrate into the flow to a distance of about 7% of the duct height. A bow shock with a downward curvature results from the interaction of the main flow with the flow entering from the first injector. Another shock which has a slight upward curvature originates just downstream of the first injector. This shock results from the flow separation over the step. Both waves reflect off the opposite wall at about the same location. Another wave is seen originating from the wall opposite the injection wall near the right-hand side of the image. This weak Mach wave originates at the end of the observation window and is used to determine the downstream Mach number. The wave angle from the observation window is 31 deg, indicating a downstream Mach number of 1.94.

In Fig. 4b, the flow is reacting, and the effects of heat release are seen. The image is distorted somewhat, especially at the entrance to the test section where all definition of the step is lost. A distortion in the height of the channel, which, due to refraction, appears reduced in the imaging plane, was corrected in the printing process by adjusting the magnification of the image. The most noticeable difference of the reacting flowfield is the thick bright line along the surface of the top wall. Although this bright line might be interpreted as the region of combustion, it is known from the OH images that will be presented later that the reaction zone penetrates much deeper into the duct than would be indicated by the bright region in the shadowgraph. This bright region most likely results from a focusing of light rays due to the strong refraction near the high-temperature injector wall.

The image in Fig. 4b reveals some important differences in the wave structure of the reacting flowfield. The waves upstream of the step appear unchanged and indicate that the step effectively isolates the nozzle from the pressure rise in the combustor. (The pressure in the base of the step at these conditions with no combustion is typically about 3.3 psia, and

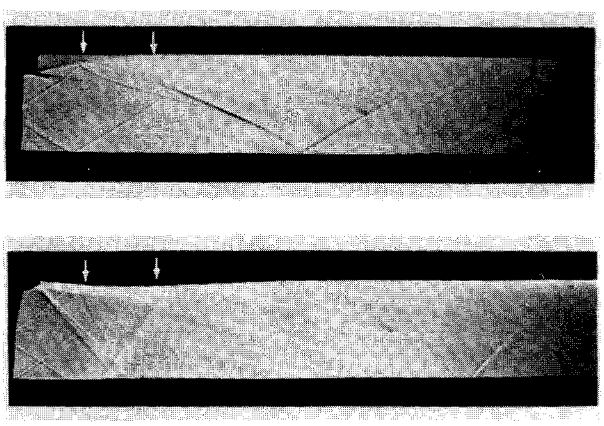

a) b)

Fig. 4 Staged injection, Q = 1.5: a) T_0 = 646 K; b) reacting, T_0 = 652 K.

about 11.2 psia with combustion.[6]) The expansion fan has been replaced by an oblique shock, which is required to match the higher step base pressure which results from the combustion. This shock is nonplanar due to the higher pressure near the side walls where there is more combustion. This three-dimensional curvature causes the oblique shock to appear as a double wave in the two-dimensional shadowgraph projection. A bow shock at the injector still exists, but at a much steeper angle. Some smearing of the waves in the reacting flow is observed that indicates some unsteadiness of the shock structure. This unsteadiness is also observed in the OH fluorescence images to be discussed later. A strong but diffuse oblique shock train is seen to originate where the shocks from the step and the first jet reach the opposite wall. The wave created at the end of the observation window has steepened to 47 deg, indicating a reduced exit Mach number of about 1.36, consistent with the addition of heat to a supersonic flow.

Broadband Visible Emission

Images of the visible broadband chemiluminescent flame emission obtained from the orientation just described are shown in Fig. 5. It is thought that this emission results from electronically excited H_2O molecules produced by the flame.[7] The images are obtained through a window in the bottom wall of the combustor. The flow direction is from bottom to top with the rearward-facing step at the lower edge of the image. The two injectors are seen as large holes along the centerline. The injector block was configured with additional side jets which were plugged for these experiments. Figures 5a–c show how the emission distribution varies with tunnel stagnation temperature. The Q-ratio was held at 1.5 for the two higher temperatures, but was reduced for the lowest temperature to avoid thermal choking. In Fig. 5a, the stagnation temperature is 741 K. A large dark region exists in the vicinity of both injectors. In the vicinity of the first injector, the dark region assumes a horseshoe shape representative of the bow shock wave. The dark region tails off about 12 step heights downstream of the step. The quartz side windows can be seen to be glowing where the gas temperature is highest on the side walls, although a slight misalignment of the camera makes it appear that the right quartz wall is hotter. The most intense emission is seen along the tunnel centerline beginning at about 12 step heights downstream of the step.

In Fig. 5b, the stagnation temperature of the air has been reduced to 581 K. The dark area associated with the two injectors is starting to separate into two distinct regions, and the total dark area is reduced in extent.

The test section is seen to continue to flamehold with the tunnel air heater turned off at a stagnation temperature of 315 K in Fig. 5c. The dark region associated with the second injector has disappeared. A horseshoe-shaped dark region is still seen at the first injector due to the bow shock wave.

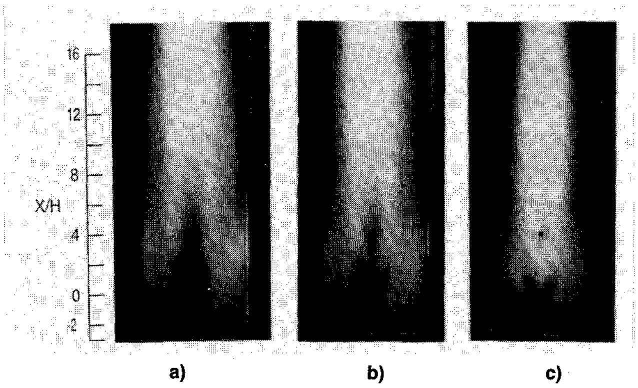

Fig. 5 Images of the visible broadband chemiluminescent flame emission: a) T_0 = 741 K, Q = 1.5; b) T_0 = 581 K, Q = 1.5; and c) T_0 = 315 K, Q = 1.0.

Recent injectant mole fraction images for this same geometry without combustion show that a significant amount of injectant exists in the center of the base of the step.[8] In this region of Figs. 5a–c, the broadband emission is greatly reduced, presumably because the mixture is too fuel rich to support combustion.

Other shadowgraphs (not shown) indicated greater penetration of the injectant flow, and therefore, greater mixing, as the stagnation temperature was reduced. The reason for this behavior is that the injectant penetration with combustion scales with an effective Q-ratio, defined using the freestream pressure and Mach number with combustion.[6] As the stagnation temperature is reduced for fixed hydrogen mass flow rate, the freestream Mach number is reduced, resulting in greater effective Q-ratios, and therefore, greater injectant penetration and mixing. If the dark regions on the emission photos indicate regions of no combustion due to insufficient mixing, then these regions would decrease as the stagnation temperature is lowered. Figure 5 is consistent with this description.

Planar Laser-Induced OH Fluorescence Visualization

Planar laser-induced fluorescence imaging of OH was performed along axial cross-sectional planes, and in longitudinal planes parallel to the main flow and the face of the injector block. The 100-ns exposure time for each video image is short enough to freeze the unsteadiness in the flow. In order to see the overall time-integrated flame structure, eight images at each position were averaged. Images of the flame cross section were obtained every two step heights beginning at one step height downstream of the step. Images of this type were averaged to show the time-integrated structure of the flame. The OH is expected to be present in superequilibrium concentrations in the reaction zones and to persist far downstream of the reaction zones due to the imbalance between the fast two-body reactions that form OH vs the slower three-body reactions that remove OH in the hydrogen-air kinetic mechanism.[9]

The first set of planar laser-induced fluorescence images, shown in Fig. 6, was collected at a position 16 step heights downstream from the first injector. The flow in these images is out of, or normal to, the page. Each image represents a cross section of the tunnel, where each of the four boundaries of the image is a wall. The top wall contains the injector block such that fuel is injected towards the bottom of the image. These time-resolved images are presented in order to show the variation in the images from shot to shot. The white regions in the images are indicative of the presence of OH. Here the Q-ratio is 1.5, the stagnation pressure is 58.0 psia, and the stagnation temperature is 672 K. The OH distribution

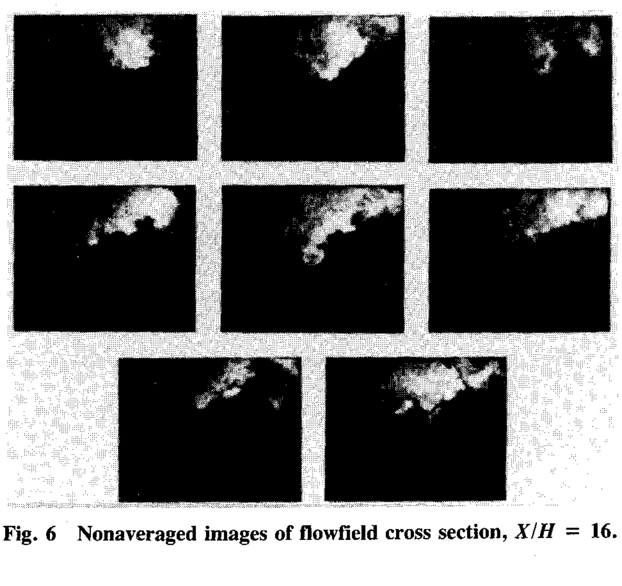

Fig. 6 Nonaveraged images of flowfield cross section, X/H = 16.

varies greatly from one 100-ns image to the next. Distinct boundaries of the OH can be observed, which would indicate that the time resolution is satisfactory for freezing flowfield details. Since the time between images is 100 ms, however, little can be said about the evolution of the turbulence between successive images. In each image, the fluorescence signal appears stronger on the right side of the image, which is the side through which the laser beam entered the tunnel. Tests showed that the asymmetry was a result of a strong absorption of the incident laser radiation by the OH, as well as by fluorescence trapping.[12]

As a first-order means of correcting for the asymmetry, the computer was used to invert the averaged image about the tunnel symmetry plane. The inverted image was averaged with the noninverted image. This method of "folding" and averaging creates a perfectly symmetrical image which is more representative of the flowfield than the raw asymmetrical images; however, the result must be interpreted strictly as a qualitative flowfield visualization, not a quantitative OH concentration distribution.

A set of folded, time-averaged, cross-sectional images obtained at 10 locations in the combustor is presented in Fig. 7. The coordinate system originates at the first injector. All dimensions have been normalized by the step height. Thus, the step is found at $X/H = -3$, the first injector at $X/H = 0$, and the second injector at $X/H = 4$. Characterization of the laser beam profile showed that the variation of the laser intensity over the regions containing OH varied no more than 30%, and thus, the fluorescence signal due to laser intensity should vary at most by 30%. Since the variation had only a small effect qualitatively, no correction for laser intensity variation was made to the images in Figs. 6 or 7.

These images offer a noticeable contrast to injectant mole fraction images presented in corresponding nonreacting studies with the same geometry.[3] Although virtually no fuel is found near the tunnel side walls in the nonreacting flowfield (except in the base recirculation zone), there is a considerable amount of OH found at the walls in the reacting flowfield. The OH also occupies a larger percentage of the duct than would be indicated by the nonreacting injectant mole fraction study. In the vicinity of the injectors and in the base of the step, there are regions of no OH signal. Apparently, the fuel-air mixture is too rich for combustion to occur here, indicating that additional mixing with the freestream is necessary for the reaction to take place.

At $X/H = -2$, the OH is confined to the region in the base of the step, and mostly near the walls, which is consistent with the mixing results.[3] As the flow moves downstream to the first injector at $X/H = 0$, there is slightly more OH penetration into the main flow. The OH is absent from the jet core where the hydrogen is insufficiently mixed with the air. In between the two injectors at $X/H = 2$, the mixture is still apparently too rich to support combustion. At $X/H = 4$, located at the second injector, the OH appears closer to the injector centerline than at the first jet. This indicates that the second jet penetrates further than the first, a result also found in the mixing studies.[3] Beginning at $X/H = 6$, the OH has filled in to the tunnel centerline. This OH pattern remains fairly constant until a location at $X/H = 14$ where the OH begins to penetrate more deeply into the flow along the centerline.

In order to show the effects of Q-ratio, the Q-ratio has been increased in Fig. 8 to 2.0. The freestream stagnation temperature and pressure have been held constant. The images at this higher Q-ratio are essentially the same as at a Q-ratio of 1.5 up to a position at $X/H = 10$. At this point, the OH begins to penetrate deeper into the flow than at a Q-ratio of 1.5. The penetration at $X/H = 16$ is 56% of the duct height at a Q-ratio of 2.0, whereas at a Q-ratio of 1.5, the penetration at $X/H = 16$ is only 47%.

The final set of images, presented in Fig. 9, was obtained with the laser sheet oriented parallel to the injector block. These images are hereafter referred to as spreading images. The images were viewed directly through the observation window at a right angle to the injector block, as shown in Fig. 3. The cylindrical lens was rotated 90 deg in order to change the orientation of the sheet. With this orientation, the effects of fluorescence trapping are reduced since the path containing

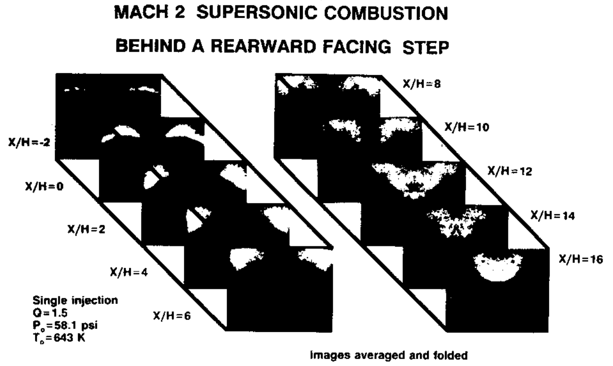

Fig. 7 Staged injection, images averaged and folded, $Q = 1.5$, $T_0 = 672$ K.

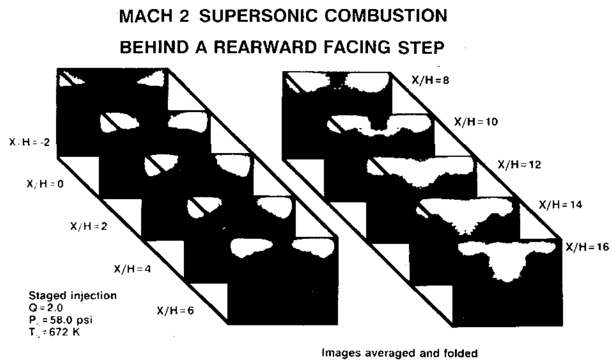

Fig. 8 Staged injection, images averaged and folded, $Q = 2.0$, $T_0 = 672$ K.

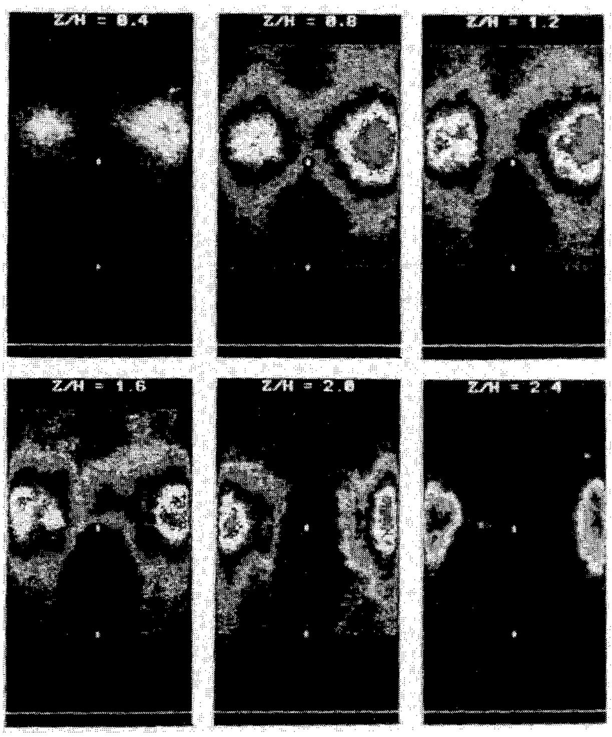

Fig. 9 Spreading images, retroreflector installed, beam correction applied, staged injection, $Q = 1.5$, $T_0 = 681$ K.

OH through which the fluorescence must travel to reach the camera is shorter. The fluorescence trapping is also symmetrical with respect to the test section centerline. This optical arrangement, therefore, allows some quantification of the amount of laser absorption that occurs as the beam passes through the flowfield.

In an attempt to reduce the image asymmetry due to beam absorption, a retroreflector was positioned at the side window where the laser sheet exited the test section. The retroreflector redirected the sheet back through the test section through the same cross-sectional plane. Since the absorption is reversed for the retroreflected beam, the effect should reduce the fluorescence asymmetry.

A drawback to the use of the retroreflector is that spatial resolution is reduced. The beam must now pass through the test section twice. With the optical system available for this experiment, it was not possible to maintain a tightly focused sheet over this greater distance. Although the sheet was no more than 0.1-mm thick at the focal point, it was as thick as 3 mm where it entered and exited the tunnel. Another limitation is that only a fraction of the unused portion of the beam is retroreflected since the beam must pass through the side window twice, and be reflected once, before it re-enters the test section. If a 4% loss is assumed for every optical surface encountered, and if 20% of the available laser radiation is absorbed on the first pass through the test section, the intensity on the re-entry side is only about 67% of the intensity at the point where the beam first enters. The beam will be absorbed by the same fraction as it passes through the test section again. After all these losses are accounted for, the beam or sheet still has 7% more intensity on the side of the tunnel through which the beam first entered. Any decrease in the optical efficiency of the windows or mirror, or increase in absorption, will increase the asymmetry of the beam intensity distribution with the retroreflector.

In these images, the light sheet intensity varied at different points. As a final step, therefore, a correction was applied to the images by normalizing the numerical value of each pixel to the measured intensity profile. The gray level corresponds to the fluorescence signal intensity.

The flow direction in Fig. 9 is from the bottom of the image to the top. The side borders of the images represent the walls of the test section, and the step and injector locations are marked on the images. Injection is directed out of the page. The Q-ratio is 1.5, the stagnation pressure is 57.6 psia, and the stagnation temperature is 681 K. Images were obtained every 2 mm, or 0.4 step heights, beginning 2 mm away from the injector block wall and ending at the location where a complete loss of signal occurred.

In the spreading images of Fig. 9, at $Z/H = 0.4$, a small amount of OH is detected just downstream and to the sides of the second injector. In the cross-sectional images, OH was found at this Z/H location at all X/H positions. In comparison with the cross-sectional images, a stronger signal level would be expected in the spreading image at this Z/H position relative to the other spreading images. Since the beam was not as tightly focused for the spreading images, however, a portion of the beam was lost at this position as a result of clipping of the beam at the side wall. This would account for the reduced signal level relative to signals observed at the other Z/H positions. In the broadband emission images of Fig. 5, the side walls are seen to glow most brightly in the region of the second injector, which is where the most intense OH fluorescence signal is found at all Z/H locations. In the area surrounding the first jet, and extending downstream to the second jet, no OH is seen. This observation is consistent with the cross-sectional OH fluorescence images and the broadband flame emission images.

At $Z/H = 0.8$, a much stronger signal is seen. Again, the strongest signal is found just downstream of the second jet, off to either side of the test section centerline. In the images in the vicinity of the first jet, the large region of no combustion is seen to persist. OH is detected, however, very close to the second jet, indicating a much smaller region around the second jet in which the fuel has not mixed sufficiently to support combustion. At about two step heights downstream of the second jet, about halfway between the second jet and the top edge of the image, OH appears to lift off the walls. This is seen also in the cross-sectional images and the broadband emission images. There is some OH that extends downstream from the second jet for about two step heights. The signal here is not as strong as the signal detected off the centerline. A similar observation can be made in the cross-sectional images where the OH has filled in behind the second jet, and at a lower intensity level.

The OH distributions at $Z/H = 1.2$ and 1.6 are similar to those found at $Z/H = 0.8$. The area surrounding the second jet which contains no OH is seen to spread laterally towards the wall as the laser sheet is moved deeper into the flow, until at $Z/H = 2.4$ the only detectable signal is at the wall. This trend is consistent with the cross-sectional images, although the actual amount of penetration of the flame into the main flow is not. In the cross-sectional images, the OH penetrates only to about $Z/H = 2.0$, whereas in the spreading images, penetration into the duct is to about $Z/H = 2.4$. This apparent deeper penetration could be partially accounted for by the reduced spatial resolution of the laser sheet used in the spreading images.

Concluding Remarks

This study involved a detailed experimental investigation of combustion in a supersonic flowfield. The results presented is the first complete flow visualization study in a reacting hydrogen-air supersonic combustor using a combination of shadowgraphs, broadband flame emission photographs, and planar laser-induced OH fluorescence images.

The shadowgraphs show that the heat release of the reaction has a strong effect on the Mach number in the combustor. When the fuel is burning, a shock is generated at the entrance of the combustor with an additional loss of total pressure. The shadowgraphs also show, as indicated by the blurring of many of the flowfield details, that heat release adds to the unsteadiness of the flow.

The shadowgraphs provide some useful information that is helpful when interpreting the OH images. Quenching of the OH fluorescence increases with pressure. The pressure rise associated with a shock would cause an increase in the amount of fluorescence quenching, and might lead to ambiguity in the vicinity of the shock as to whether OH actually exists behind a shock, or whether it has just been quenched. The shadowgraphs of the reacting flowfield show that most of the shock structure has disappeared from the region of combustion. It can be safely assumed that any sharp diminishing of OH signals observed is not the result of shock quenching of the fluorescence, but of insufficient mixing.

The 35-mm photographs of the broadband emission of the flame show that for the high stagnation temperature test conditions there is a region downstream of the first fuel injector where no combustion occurs. This is also seen in the OH visualization images. As the stagnation temperature is reduced, this area of no reaction closes in on the injector jets. Other shadowgraphs have shown that as the stagnation temperature is reduced, the penetration of the transverse jets increases. This behavior is consistent with an increase in the effective Q-ratio with combustion and correspondingly increased fuel penetration and mixing. The increased mixing associated with the increased penetration at the lower stagnation temperature could cause the region of combustion to move closer to the injector cores.

The planar OH fluorescence images of the reacting flowfield provide an interesting contrast to earlier studies of the corresponding nonreacting flowfield. Although it was previously recognized that streamwise vorticity would be largely responsible for mixing in a supersonic combustor of this configuration, it appears that mixing may be affected more by the heat release. Apparently a pressure rise associated with the heat release involved in the reaction forces a rapid lateral displacement of the fuel towards the side walls. A large amount of burning, therefore, occurs on the side walls. This would suggest that the mixing distributions observed in the nonreacting flowfield have been greatly altered. The walls limit the amount of spreading that would otherwise occur, and possibly induce some recirculation or deceleration of the flow which could aid in flameholding. No OH is observed in the OH images in the regions surrounding the injector jets. These regions are apparently too fuel rich to support combustion or too cold for positive emission.

This study brings to light a number of problems that must be dealt with before planar laser-induced OH spectroscopy can be successfully employed for a complete quantitative investigation of a supersonic reacting flowfield. These problems are outlined in the Appendix.

Appendix

Laser-beam absorption, fluorescence quenching, and fluorescence trapping all affect the interpretation of the images in this study. It is seen from Eq. (2) that to relate the fluorescence signal to a flowfield variable on the right side of the equation, values for the other flowfield variables in the equation must be known, or else eliminated. As mentioned earlier, if a transition is selected that is insensitive to temperature, the fluorescence signal becomes proportional to the number density of the molecule and inversely proportional to the quenching term Q. Q is given by the following expression:

$$Q = \sum_i n_i v_i \sigma_i(T, N_i)$$

where n_i is the number density of the collision specie, v_i is the relative collision velocity, σ_i is the quenching cross section, T is the temperature, and N_i is the rotational quantum number without spin coupling. The number density n_i of the collision specie is given by

$$n_i = (Py_i/kT)$$

where P is the local pressure, k is Boltzmann's constant, and y_i is the mole fraction of the collision specie. The relative collision velocity is given by

$$v = \sqrt{(8kT/\pi M)}$$

where M is the reduced mass given by

$$M = \frac{m_{OH} m_i}{m_{OH} + m_i}$$

where m_{OH} and m_i are the masses of the OH molecule and the colliding specie, respectively.

If only one major collision specie is assumed, e.g., H_2O, the summation can be dropped, and the relation for the fluorescence signal becomes

$$S_f \propto \frac{1}{Q} F_1 N_0 \propto \frac{T}{Py} \frac{1}{\sqrt{T}} \frac{1}{\sigma} F_1 n_0 \propto \frac{N_o \sqrt{T}}{Py\sigma} F_1$$

From this relation, it can be seen that in order to directly relate the fluorescence intensity to a quantitative value for number density, the temperature, pressure, collisional cross section (which is a strong function of temperature), and mole fraction of the collision partner must be known. In a supersonic combustion flowfield, these values can vary widely.

As an example, consider flow across a normal shock in a chemically reacting Mach 2 flow. Since the chemical kinetics require many collisions to adjust, the gas composition is essentially frozen across the wave and the ratio of property values across the wave is given by the constant specific heat ratio Rankine-Hugoniot jump relations. The temperature across this shock is predicted to increase by a factor of 1.688 and the pressure by 4.500. The OH number density should, therefore, increase by 2.667. The above equation predicts that the fluorescence signal will drop to 77% of the upstream value, provided that a transition was used that is insensitive to temperature. Thus, the ratio of the actual OH number density across the shock to that inferred by assuming fluorescence intensity proportional to OH number density is 3.46.

Absorption of the laser beam and trapping of the fluorescence signal were shown to significantly affect the intensity of the signal that is actually detected by the camera. The degree of the effect is not easily determined, and is sufficient to preclude deducing any meaningful quantitative thermodynamic information. Other studies have shown that as much as 20% of the beam could be absorbed across the test section used in this study, and as much as 20% of the fluorescence signal could be trapped, depending on the point of origin of the signal.[10]

This Appendix shows that the fluorescence signal level cannot be used directly to quantitatively evaluate OH number density in a supersonic combustor due to fluorescence quenching. The fluorescence signal is still useful qualitatively in that the signal does positively indicate the presence of OH. Future studies must address the problems associated with quenching as well as absorption of the incident radiation and trapping of the emitted fluorescence before a quantitative investigation using laser-induced fluorescence can be completed.

Acknowledgments

This work was supported by NASA Grants NAG 1-795 and NGT-50142 from NASA Langley Research Center, G. Burton Northam, technical monitor.

References

[1]Uenishi, K., Rogers, R. C., and Northam, G. B., "Numerical Predictions of a Rearward-Facing-Step Flow in a Supersonic Combustor," *Journal of Propulsion and Power*, Vol. 5, No. 2, 1989, pp. 158–164.

[2]Chitsomboon, T., Northam, G. B., Rogers, R. C., and Diskin, G. S., "CFD Prediction of the Reacting Flowfield Inside a Subscale Scramjet Combustor," AIAA Paper 88-3259, July 1988.

[3]Abbitt, J. D., III, Hartfield, R. J., and McDaniel, J. C., "Mole Fraction Imaging of Transverse Injection in a Ducted Supersonic Flow," *AIAA Journal*, Vol. 29, No. 3, 1991, pp. 431–435.

[4]Hartfield, R. J., Jr., Hollo, S. D., and McDaniel, J. C., "Planar Temperature Measurement in Compressible Flows Using Laser-Induced Iodine Fluorescence," *Optics Letters*, Vol. 16, No. 2, 1991, pp. 106–108.

[5]Abbitt, J. D., III, "Flow Visualization of Supersonic Flow Through a Combustor Section," Ph.D. Dissertation, Univ. of Virginia, Charlottesville, VA, 1991.

[6]Segal, C., "Experimental and Numerical Investigation of Hydrogen Combustion in a Supersonic Flow," Ph.D. Dissertation, Univ. of Virginia, Charlottesville, VA, 1991.

[7]Engel, V., Meijer, G., Bath, A., Anderson, P., and Schinke, R., "The $C \rightarrow A$ Emission in Water: Theory and Experiment," *Journal of Chemical Physics*, Vol. 87, No. 8, 1987, pp. 4310–4314.

[8]Hartfield, R. J., Hollo, S. D., and McDaniel, J. C., "Planar Measurement of Flow Field Parameters in a Nonreacting Supersonic Combustor Using Laser-Induced Iodine Fluorescence," AIAA Paper 90-0162, Jan. 1990.

[9]Hitch, B. D., and Senser, D. W., "Reduced H_2-O_2 Mechanisms for use in Reacting Flow Simulation," AIAA Paper 88-0732, Jan. 1988.

[10]Laufer, G., Quagliaroli, T. M., Krauss, R. H., and McDaniel, J. C., "Evaluation of OH Laser-Induced Fluorescence Techniques for Supersonic Combustion Diagnostics," AIAA Paper 92-0508, Jan. 1992.